Title

Small-conductance Ca^{2+}-activated K^{+} channels promote J-wave syndrome and phase 2 reentry.

Journal

Heart rhythm, 17(9)

ISSN

1547-5271

Authors

Landaw, Julian
Zhang, Zhaoyang
Song, Zhen
et al.

Publication Date

2020-09-01

DOI

10.1016/j.hrthm.2020.04.023

Peer reviewed

HHS Public Access

Author manuscript

Heart Rhythm. Author manuscript; available in PMC 2021 September 01.

Published in final edited form as:

Heart Rhythm. 2020 September ; 17(9): 1582–1590. doi:10.1016/j.hrthm.2020.04.023.

Small-conductance Ca^{2+}-activated K^+ channels promote J-wave syndrome and phase-2 reentry

Julian Landaw, PhD[1,#], **Zhaoyang Zhang, PhD**[1,#], **Zhen Song, PhD**[1], **Michael B. Liu, PhD**[1], **Riccardo Olcese, PhD**[2,3], **Peng-Sheng Chen, MD**[5], **James N. Weiss, MD**[1,3], **Zhilin Qu, PhD**[1,4,*]

[1]Department of Medicine, David Geffen School of Medicine, University of California, Los Angeles, California 90095, USA

[2]Department of Anesthesiology and Perioperative Medicine, David Geffen School of Medicine, University of California, Los Angeles, California 90095, USA

[3]Department of Physiology, David Geffen School of Medicine, University of California, Los Angeles, California 90095, USA

[4]Department of Computational Medicine, David Geffen School of Medicine, University of California, Los Angeles, California 90095, USA

[5]Krannert Institute of Cardiology and Division of Cardiology, Department of Medicine, Indiana University School of Medicine, Indianapolis, Indiana 46202, USA

Abstract

Background—Small-conductance calcium (Ca^{2+})-activated potassium (SK) channels play complex roles in cardiac arrhythmogenesis. SK channels colocalize with L-type Ca^{2+} channels, yet how this colocalization affects cardiac arrhythmogenesis is unknown.

Objective—To investigate the role of colocalization of SK channels with L-type Ca^{2+} channels in promoting J-wave syndrome and ventricular arrhythmias.

Methods—We carried out computer simulations of single-cell and tissue models. SK channels in the model were assigned to preferentially sense Ca^{2+} in the bulk cytosol, subsarcolemmal space, or junctional cleft.

Results—When the SK channels sense Ca^{2+} in the bulk cytosol, the SK current (I_{SK}) rises and decays slowly during an action potential, the action potential duration (APD) decreases as the maximum conductance increases, no complex APD dynamics and phase-2 reentry can be induced by I_{SK}. When the SK channels sense Ca^{2+} in the subsarcolemmal space or the junctional cleft, I_{SK}

*Correspondence to: Zhilin Qu, PhD, Department of Medicine, Division of Cardiology, David Geffen School of Medicine at UCLA, A2-237 CHS, 650 Charles E. Young Drive South, Los Angeles, CA 90095, zqu@mednet.ucla.edu.
#JL and ZZ contribute equally

Disclosures

None.

can rise and decay rapidly during an action potential in a spike-like pattern due to spiky Ca^{2+} transients in these compartments, which can cause spike-and-dome action potential morphology, APD alternans, J-wave elevation, and phase-2 reentry. Our results can account for the experimental finding that activation of I_{SK} induced J-wave syndrome and phase-2 reentry in rabbit hearts.

Conclusions—Colocalization of SK channels with L-type Ca^{2+} channels so that they preferentially sense Ca^{2+} in the subsarcolemmal or junctional space may result in a spiky I_{SK}, which can functionally play a similar role of I_{to} in promoting J-wave syndrome and ventricular arrhythmias.

Keywords

SK channel; J-wave syndrome; alternans; phase-2 reentry; computer modeling

Introduction

Small-conductance Ca^{2+}-activated K^+ (SK) channels are widely expressed in a variety of cell types and play multiple biological roles, particularly in the nervous system where they regulate neuronal firing.[1] The SK current (I_{SK}) is also present in atrial and ventricular myocytes under normal and diseased conditions.[2–9] Depending on experimental conditions, both proarrhythmic and antiarrhythmic effects of I_{SK} have been identified in experiments using apamin, a selective SK channel blocker. However, the underlying mechanisms are not well understood.

I_{SK} is activated by intracellular Ca^{2+} with a fast time constant on the order of a few milliseconds,[10–13] and thus its rising and decaying time course tracks the intracellular Ca^{2+} transient. Moreover, studies have found that SK channels colocalize with L-type Ca^{2+} channels (LCCs) in ventricular myocytes [4, 5, 7] such that the SK channels may be transiently exposed to a much higher Ca^{2+} in the submembrane space when the nearby LCCs and ryanodine receptors (RyRs) open. This may make I_{SK} a transient current, similar to the transient outward K^+ current (I_{to}). In agreement with this view, spike-like I_{SK} has been observed in ventricular myocytes under voltage clamp conditions.[7, 14] In a recent experimental study, Chen et al[15] discovered that rabbit hearts exposed to a drug that activates I_{SK} while simultaneously inhibiting the Na^+ current (INa) developed a J-wave syndrome leading to phase-2 reentry (P2R) and ventricular arrhythmias. Since I_{to}, the current most commonly implicated in P2R, is very small in rabbits at normal heart rates, we hypothesized that the arrhythmogenic J-wave syndrome in the rabbit hearts was related to the I_{to}-like properties of the activated I_{SK}.

To test this hypothesis, we carried out computer simulations of single myocyte and one-dimensional (1D) cable models to investigate the effects of I_{SK} and its subcellular localization on action potential (AP) morphology and P2R. In single myocytes, we investigated the influence of the subcellular localization of SK channels on AP morphology and complex action potential duration (APD) dynamics. In 1D cable simulations, we simulated the effects of I_{SK} and its subcellular localization on J-wave properties and P2R. Our main conclusion is that colocalization of the SK channels with the LCCs results in I_{SK}

properties that can result in J-wave syndrome and potentiate ventricular arrhythmias via promoting T-wave alternans and P2R.

Methods

Modeling I_{SK}

Komendantov et al[16] used a I_{SK} formulation to study neuronal firing as follows:

$$I_{SK} = G_{SK}\frac{1}{1+\left(\frac{K_d}{[Ca]}\right)^4}(V - E_K)\,. \tag{1}$$

Here we modified the I_{SK} formulation of Komendantov et al to include a time-dependent gating variable, i.e.,

$$I_{SK} = G_{SK}x_{SK}(V - E_K) \tag{2}$$

where G_{SK} is the maximum conductance and E_K the K^+ reversal potential. x_{SK} is the time-dependent gating variable described by

$$\frac{dx_{SK}}{dt} = \frac{x_{SK,\infty} - x_{SK}}{\tau_{SK}} \tag{3}$$

where $x_{SK,\infty}$ is a Hill function of Ca^{2+}, i.e.,

$$x_{SK,\infty} = \frac{1}{1+\left(\frac{K_d}{[Ca]_{SK}}\right)^n} \tag{4}$$

where $[Ca^{2+}]_{SK}$ is the Ca^{2+} concentration sensed by SK channels. In Eq.4, n is the Hill coefficient, which we set at n=4, in the range from 2 to 6 as measured in experiments.[3, 10–13, 17] Thus when τ_{sk}=0, Eq.2 is identical to Eq.1. The reported experimental K_d is in the sub-μM range.[3, 10–13, 17] For example, Chua et al[3] found K_d=0.5 μM for normal ventricle and K_d=0.3 μM for failing ventricles. However, we will use different K_d for the different SK localizations, as discussed in more detail in the Discussion section.

As for τ_{sk}, we plotted experimental data in Fig. 1 from different experiments (in different symbols).[10–13] Using their multi-state Markovian SK channel model, Hirschberg et al[10] showed that τ_{sk} exhibits an inverse linear relationship with $[Ca^{2+}]$. In other words, τ_{sk} can be represented by a Hill function with Hill coefficient of 1. Based on this observation, we formulated τ_{sk} as

$$\tau_{SK} = \tau_0 + \frac{\tau_1}{1+\frac{[Ca]_{SK}}{0.1}} \tag{5}$$

A plot of this function for τ_0=4 and τ_1=20 is shown in Fig.1, which is well within the range of the experimental data.

In this study, we used the Shannon-Bers rabbit ventricular AP model[18] which has three cytosolic Ca^{2+} compartments: bulk cytosolic compartment, subsarcolemmal compartment, junctional cleft. The corresponding Ca^{2+} concentrations in the three compartments are abbreviated as $[Ca^{2+}]_i$, $[Ca^{2+}]_{SL}$, and $[Ca^{2+}]_{jct}$, respectively. These concentrations will be used for $[Ca^{2+}]_{SK}$ in Eqs.4 and 5 when the SK channels sense Ca^{2+} in the different compartments.

Single-cell model

Simulations of single cells were carried out using the following differential equation:

$$C_m \frac{dV}{dt} = -I_{ion} + I_{sti} \tag{6}$$

where V is the voltage and C_m=1 μF/cm^2 is the membrane capacitance. The ionic current I_{ion} was from the Shannon-Bers rabbit ventricular AP model,[18] with the original Matlab code downloaded from the website: https://somapp.ucdmc.ucdavis.edu/Pharmacology/bers/.

1D cable model

1D cables were described by the following partial differential equation for voltage:

$$\frac{\partial V}{\partial t} = -\frac{I_{ion}}{C_m} + D\frac{\partial^2 V}{\partial x^2} \tag{7}$$

where D=0.001 cm^2/ms is the diffusion constant describing the strength of gap junction coupling. The pseudo-ECG was calculated as:

$$ECG = \int_0^{3\ cm} \mathrm{D}\,\nabla V \cdot \nabla\left(\frac{1}{r}\right) dx \tag{8}$$

where $r = \sqrt{(x - x_p)^2 + y_p^2}$ and x is a point in the cable and (x_p,y_p)=(2.28 cm, 1 cm) is the location of the pseudo-ECG electrode.

Numerical methods

Single cell simulations were performed using a forward Euler method with a fixed time step Δt = 0.005 ms. 1D cable simulations were performed using CUDA, a programming language designed for graphical processing units, and a forward Euler method with a fixed time step Δt = 0.005 ms. The cable consists of 200 cells, and the cell length corresponding to the spatial step is Δx = 0.015 cm. No-flux boundary conditions were used.

Results

SK channel localization and I_{SK} properties

Figs.2 A–C show an AP and the corresponding Ca^{2+} transients from the different cytosolic compartments of the Shannon-Bers model. The bulk cytosolic Ca^{2+} transient peaks at 0.5 μM (Fig.2A), the subsarcolemmal Ca^{2+} peaks at 8 μM and becomes spikier (Fig.2B), and the junctional Ca^{2+} reaches as high as 150 μM and is much spikier (Fig.2C). We then

investigated the effects of SK channel localization on I_{SK} properties under an AP clamp condition using the AP waveform in Fig.2A. Figs.2 D–F show I_{SK} versus time for different K_d (upper panels) and peak I_{SK} versus K_d (lower panels) for SK channels sensing Ca^{2+} in different compartments, labeled as SK-$[Ca^{2+}]_i$, SK-$[Ca^{2+}]_{SL}$, and SK-$[Ca^{2+}]_{jct}$, respectively. When the SK channels sense Ca^{2+} in the bulk cytosolic compartment, I_{SK} is broad and the amplitude decreases by half when the K_d increases to 0.5 μM. When the SK channels sense Ca^{2+} in the subsarcolemmal compartment, I_{SK} is broad when the K_d is low but becomes narrower as the K_d increases. The amplitude of I_{SK} does not decrease until the K_d reaches 2 μM and by half when the K_d increases to 7.5 μM. When the SK channels sense Ca^{2+} in the junctional cleft, I_{SK} behaves similarly to when the SK channels sense Ca^{2+} in the subsarcolemmal compartment. However, a much higher K_d is required. The amplitude of I_{SK} does not decrease until K_d increases to 10 μM and by half when the K_d increases to 90 μM. Note that the current densities and width of the current profiles in Figs.2 E and F are in the same ranges as the experimental data shown by Terentyev et al.[7, 14]

Effects of I_{SK} on AP morphology

We next carried out simulations to show how I_{SK} properties affect the AP morphology (Fig.3). When the K_d is low (upper panels in Fig.3), increasing G_{SK} shortens APD and the AP becomes more and more triangular for the SK channels sense Ca^{2+} in anyone of the three compartments. When the SK channels sense Ca^{2+} in the bulk cytosolic compartment, changing the K_d does not change the AP properties. However, when the SK channels sense Ca^{2+} in the subsarcolemmal compartment or the junctional cleft, spike-and-dome morphology and lengthening of APD occur when G_{SK} was increased to a certain value. When G_{SK} increases further, the APD suddenly shortens to a very short value. These AP behaviors are the same as those induced by I_{to} as shown in many of the previous studies.[19–21]

I_{SK} promotes APD alternans and chaos

We examined the effects and the subcellular localization of SK channels on APD dynamics (Fig.4). When the K_d is low, increasing G_{SK} decreases APD but the AP is always stable independent of the SK channel localization. When the SK channels sense Ca^{2+} in the bulk cytosolic compartment, changing the K_d does not induce any complex AP dynamics. But when the SK channels sense Ca^{2+} in the subsarcolemmal compartment or the junctional cleft and the K_d is large so that I_{SK} is spiky, APD alternans and more complex APD dynamics occur. Notably, these types of APD dynamics can also be induced by I_{to} as previously demonstrated in both computational and experimental studies.[20–23]

I_{SK} promotes J-wave syndrome and P2R

To examine whether I_{SK} can promote J-wave syndrome and P2R in tissue, we simulated 1D cables of 200 cells. Heterogeneity was simulated by increasing G_{SK} in half of the cable. The cable was paced from the endocardial side (top) and pseudo-ECGs were recorded on the epicardial side (bottom). When the SK channels sense Ca^{2+} in the bulk cytosolic compartment (Fig.5A), increasing G_{SK} results in a large upright T-wave but only has a small effect on elevating the J-point. Changing the K_d does not affect this behavior. When the SK channels sense Ca^{2+} in the subsarcolemmal compartment or the junctional cleft, if the K_d is

low, we also observed the same behavior. However, when the K_d is large (Figs.5 B and C), increasing G_{SK} elevates the J-point and eventually promotes P2R. Note that in addition to elevation of the J-point, the ECG becomes coved, which is a characteristic ECG behavior in Brugada syndrome.[24]

We scanned G_{SK}, K_d, and τ_{SK} for P2R in the 1D cable model. When the SK channels sense Ca^{2+} in the bulk cytosolic compartment, we cannot find P2R in this 1D cable model. When the SK channels sense Ca^{2+} in the subsarcolemmal compartment (Fig.6A) or the junctional cleft (Fig.6B), P2R can be observed for certain combinations of the two parameters. P2R is suppressed by increasing the activation time constant (Figs. 6 C and D).

Discussion

I_{SK} is present in both atrial and ventricular myocytes under normal and diseased conditions2, [3, 6, 8, 9] and has been shown to be proarrhythmic in some settings and antiarrhythmic in others.[3, 6, 8, 9, 25, 26] Recently, pharmacologic I_{SK} activation with simultaneous I_{Na} suppression was shown to induce a J-wave syndrome leading to ventricular arrhythmias in isolated rabbit hearts.[15] Although I_{to} is thought to play a key role in J-wave syndrome,[24] rabbits have almost no I_{to} at physiological heart rates due to its slow recovery from inactivation. This suggests that I_{SK} may have substituted for I_{to} due to its similar transient behavior as it tracks the intracellular Ca^{2+} transient. In this study, we used computer modeling to investigate the conditions under which I_{SK} may substitute for I_{to} to produce I_{to}'s hallmark arrhythmogenic features of spike-and-dome AP morphologies,[19–21] APD alternans, complex APD dynamics,[21–23] and P2R in cardiac tissue.[27–29] We show that when the SK channels sense Ca^{2+} in the subsarcolemmal or the junctional spaces where intracellular Ca^{2+} transient is spiky, I_{SK} rises and decays rapidly like I_{to} to promote J-wave syndrome and P2R.

Thus, our study provides mechanistic insight into the experimental findings reported in isolated rabbit hearts that I_{SK} induced an arrhythmogenic J-wave syndrome, despite the functional absence of significant I_{to}. The results from our study suggests that I_{SK} may synergize with I_{to} to cause all-or-none early repolarization and its arrhythmogenic consequences in human early repolarization syndromes such as the Brugada syndrome. Most of the experimental studies of P2R have been carried out in canine hearts[23, 27, 30] which have an unusually high I_{to} density in the right ventricular epicardium. Experimentally, P2R has been much more difficult to induce in other species. For example, Park et al[31] attempted unsuccessfully to create a pig model of Brugada syndrome by engineering a human-homologous loss-of-function SCN5A mutation, suggesting that I_{to} density in the pig was not high enough to recapitulate the Brugada syndrome phenotype. Therefore, in the setting of low or reduced I_{to}, activation of I_{SK} can promote J-wave syndrome and arrhythmias, as in the rabbit experiments by Chen et al.[15]

Limitations

Several limitations are worth mentioning. Our simulations show that J-wave syndrome and P2R occur when the SK channels sense Ca^{2+} in the junctional cleft or the submembrane space such that they are transiently exposed to much higher [Ca^{2+}] when LCCs and RyRs

open. However, our simulations also show that in order to produce a spiky enough I_{SK} for P2R, a higher K_d than experimentally estimated values in the sub-μM range is required. [3, 10–13, 17] K_d is the Ca^{2+} concentration at which I_{SK} is half-maximally activated, and thus a lower K_d indicates that the SK channel is more sensitive to Ca^{2+}. Since the Ca^{2+} concentrations in the junctional cleft or the subsarcolemmal space is much higher than 1 μM, I_{SK} amplitude may become saturated during the AP if the K_d is in the sub-μM range (see Fig.2), blunting the spikiness too much for J-wave elevation and P2R to occur. However, experimental studies by Terentyev et al have shown that I_{SK} is much spikier than the bulk Ca^{2+} transient [7, 14]. Possible explanations are that: 1) the actual K_d of SK channels in cardiac myocytes is higher than the measured apparent K_d assessed from bulk Ca^{2+} concentration, perhaps due to modulation of the K_d by accessory proteins in the junctional cleft, or 2) I_{SK} is activated by sub-μM and then inactivated by supra-μM Ca^{2+} concentration levels in the submembrane or junctional cleft. Evidence of inactivation or inhibition of I_{SK} at supra-μM Ca^{2+} has been demonstrated in experiments.[14, 32]

Furthermore, simulation results can be model specific, and we only used the Shannon-Bers model in this study. For example, our simulations could substantially overestimate the K_d due to the very high Ca^{2+} concentrations in the junctional cleft or the subsarcolemmal space of the model. In an experimental study of rabbit ventricular myocytes by Weber et al [33], the measured Ca^{2+} concentration in the subsarcolemmal space is about 3- to 4-fold higher than the bulk cytosolic Ca^{2+} concentration. However, in the Shannon-Bers model, the subsarcolemmal Ca^{2+} concentration is 16-fold higher and the junctional cleft Ca^{2+} concentration is 300-fold higher than the bulk Ca^{2+} concentration (see Fig.2). This may result in a several-fold overestimation of the critical K_d for P2R.

Another limitation is that the I_{SK} conductance needed for P2R in our simulations is much larger than experimentally measured values in ventricular myocytes under physiological or pathophysiological conditions.[3, 14, 34] This raises an issue whether I_{SK} was indeed responsible for P2R in the rabbit experiments by Chen et al.[15] One possibility is that in these experiments I_{SK} was activated by drugs, which could be strong enough for P2R to occur. Another plausible explanation is that besides I_{SK}, there are other outward transient currents, which combine additively with I_{SK} to result in a total transient outward current that is strong enough to potentiate P2R. For example, experimental measurements show that the Ca^{2+}-activated chloride current (I_{Cl}) is also a spiky transient outward current,[34, 35] and is present in pig and rabbit ventricular myocytes. Therefore, I_{SK} alone may be not strong enough to induce P2R in the rabbit experiments by Chen et al, but it may combine with I_{Cl} to potentiate P2R. To demonstrate this possibility, we carried out the same 1D cable simulations as in Figs.5 and 6, and showed that increasing G_{Cl} decreased the G_{SK} threshold for P2R (Fig.7), indicating that the two currents are complementary to each other in promoting P2R. Similar to the limitations for the critical K_d discussed above, the critical current magnitude for P2R may also be model-dependent, which needs to be validated by simulations of other models or by real experiments.

Nevertheless, the key property that I_{SK} is able to promote J-wave syndrome and ventricular arrhythmias is its spike-like behavior, which has indeed been shown in experimental measurements in ventricular myocytes.[7, 14, 34] The spikiness of I_{SK} may depend on many

factors, such as Ca^{2+} transient profile, SK channel localization, K_d of SK channel activation, and activation time constant. The insights from our simulations provide a potential mechanism of J-wave syndrome and arrhythmogenesis in the experiments by Chen et al[15] and may be helpful for further experiments to reveal the roles of I_{SK} in promoting J-wave syndrome and arrhythmogenesis.

Conclusions

SK channels, which colocalize with LCCs in ventricular myocytes, may give rise to a spike-like I_{SK} due to the SK channels sensing a spiky Ca^{2+} transient in the junctional cleft or subsarcolemmal space. I_{SK} can functionally play the role of I_{to} or combine together with other transient outward currents, such as I_{to} or I_{Cl}, to result in J-wave syndrome and potentiate ventricular arrhythmias by promoting T-wave alternans and P2R.

Acknowledgments

Funding Sources

This work was supported by National Institutes of Health, under Grants No. R01 HL139829, R01 HL134709, R01 HL134346 (to R.O.), T32-GM008185 (to J. L. and M.B.L), F30 HL140864 (to J.L.), and F30 HL132449 (to M.B. L.), the Laubisch and Kawata Endowments of UCLA (to J.N.W.) and a Medtronic-Zipes Endowment of the Indiana University (to P.-S.C.), and Natural Science Foundation of Ningbo, China under Grant No. 2017A610142 (to Z.Z.).

References

1. Adelman JP, Maylie J, Sah P. Small-Conductance Ca2+-Activated K+ Channels: Form and Function. Annu Rev Physiol. 2012;74:245–269. [PubMed: 21942705]
2. Tuteja D, Xu D, Timofeyev V, et al. Differential expression of small-conductance Ca2+-activated K + channels SK1, SK2, and SK3 in mouse atrial and ventricular myocytes. American Journal of Physiology - Heart and Circulatory Physiology. 2005;289:H2714–H2723. [PubMed: 16055520]
3. Chua SK, Chang PC, Maruyama M, et al. Small-conductance calcium-activated potassium channel and recurrent ventricular fibrillation in failing rabbit ventricles. Circ Res. 2011;108:971–979. [PubMed: 21350217]
4. Lu L, Zhang Q, Timofeyev V, et al. Molecular Coupling of a Ca2+-Activated K+ Channel to L-Type Ca2+ Channels via a-Actinin2. Circ Res. 2007;100:112–120. [PubMed: 17110593]
5. Zhang X-D, Coulibaly ZA, Chen WC, et al. Coupling of SK channels, L-type Ca2+ channels, and ryanodine receptors in cardiomyocytes. Scientific Reports. 2018;8:4670. [PubMed: 29549309]
6. Chang PC, Turker I, Lopshire JC, et al. Heterogeneous upregulation of apamin-sensitive potassium currents in failing human ventricles. J Am Heart Assoc. 2013;2:e004713. [PubMed: 23525437]
7. Terentyev D, Rochira JA, Terentyeva R, Roder K, Koren G, Li W. Sarcoplasmic reticulum Ca2+ release is both necessary and sufficient for SK channel activation in ventricular myocytes. Am J Physiol Heart Circ Physiol. 2014;306:H738–H746. [PubMed: 24381116]
8. Chang P-C, Hsieh Y-C, Hsueh C-H, Weiss JN, Lin S-F, Chen P-S. Apamin induces early afterdepolarizations and torsades de pointes ventricular arrhythmia from failing rabbit ventricles exhibiting secondary rises in intracellular calcium. Heart Rhythm. 2013;10:1516–1524. [PubMed: 23835258]
9. Zhang X-D, Lieu DK, Chiamvimonvat N. Small-conductance Ca2+-activated K+ channels and cardiac arrhythmias. Heart Rhythm. 2015;12:1845–1851. [PubMed: 25956967]
10. Hirschberg B, Maylie J, Adelman JP, Marrion NV. Gating of Recombinant Small-Conductance Ca-activated K+ Channels by Calcium. The Journal of General Physiology. 1998;111:565–581. [PubMed: 9524139]
11. Xia XM, Fakler B, Rivard A, et al. Mechanism of calcium gating in small-conductance calcium-activated potassium channels. Nature. 1998;395:503. [PubMed: 9774106]

12. Bildl W, Strassmaier T, Thurm H, et al. Protein Kinase CK2 Is Coassembled with Small Conductance Ca2+-Activated K+ Channels and Regulates Channel Gating. Neuron. 2004;43:847–858. [PubMed: 15363395]
13. Pedarzani P, Mosbacher J, Rivard A, et al. Control of Electrical Activity in Central Neurons by Modulating the Gating of Small Conductance Ca2+-activated K+ Channels. J Biol Chem. 2001;276:9762–9769. [PubMed: 11134030]
14. Hamilton S, Polina I, Terentyeva R, et al. PKA phosphorylation underlies functional recruitment of sarcolemmal SK2 channels in ventricular myocytes from hypertrophic hearts. The Journal of Physiology. 2019;0.
15. Chen M, Xu D-Z, Wu AZ, et al. Concomitant SK current activation and sodium current inhibition cause J wave syndrome. JCI Insight. 2018;3:e122329.
16. Komendantov AO, Komendantova OG, Johnson SW, Canavier CC. A Modeling Study Suggests Complementary Roles for GABAA and NMDA Receptors and the SK Channel in Regulating the Firing Pattern in Midbrain Dopamine Neurons. J Neurophysiol. 2004;91:346–357. [PubMed: 13679411]
17. Hirschberg B, Maylie J, Adelman JP, Marrion NV. Gating Properties of Single SK Channels in Hippocampal CA1 Pyramidal Neurons. Biophys J. 1999;77:1905–1913. [PubMed: 10512811]
18. Shannon TR, Wang F, Puglisi J, Weber C, Bers DM. A mathematical treatment of integrated Ca dynamics within the ventricular myocyte. Biophys J. 2004;87:3351–3371. [PubMed: 15347581]
19. Greenstein JL, Wu R, Po S, Tomaselli GF, Winslow RL. Role of the calcium-independent transient outward current I(to1) in shaping action potential morphology and duration. Circ Res. 2000;87:1026–1033. [PubMed: 11090548]
20. Clancy CE, Rudy Y. Na(+) channel mutation that causes both Brugada and long-QT syndrome phenotypes: a simulation study of mechanism. Circulation. 2002;105:1208–1213. [PubMed: 11889015]
21. Landaw J, Qu Z. Memory-induced nonlinear dynamics of excitation in cardiac diseases. Physical Review E. 2018;97:042414. [PubMed: 29758700]
22. Lukas A, Antzelevitch C. Differences in the electrophysiological response of canine ventricular epicardium and endocardium to ischemia. Role of the transient outward current. Circulation. 1993;88:2903–2915. [PubMed: 8252704]
23. Morita H, Zipes DP, Lopshire J, Monta ST, Wu J. T wave alternans in an in vitro canine tissue model of Brugada syndrome. Am J Physiol Heart Circ Physiol. 2006;291:H421–428. [PubMed: 16648179]
24. Antzelevitch C, Yan G-X, Ackerman MJ, et al. J-Wave syndromes expert consensus conference report: Emerging concepts and gaps in knowledge. Heart Rhythm. 2016;13:e295–e324. [PubMed: 27423412]
25. Kennedy M, Bers DM, Chiamvimonvat N, Sato D. Dynamical effects of calcium-sensitive potassium currents on voltage and calcium alternans. The Journal of Physiology. 2017;595:2285–2297. [PubMed: 27902841]
26. Morotti S, Koivumäki JT, Maleckar MM, Chiamvimonvat N, Grandi E. Small-Conductance Ca2+-Activated K+ Current in Atrial Fibrillation: Both Friend and FOE. Biophys J. 2016;110:274a.
27. Lukas A, Antzelevitch C. Phase 2 reentry as a mechanism of initiation of circus movement reentry in canine epicardium exposed to simulated ischemia. Cardiovasc Res. 1996;32:593–603. [PubMed: 8881520]
28. Maoz A, Christini DJ, Krogh-Madsen T. Dependence of phase-2 reentry and repolarization dispersion on epicardial and transmural ionic heterogeneity: a simulation study. Europace. 2014;16:458–465. [PubMed: 24569901]
29. Bueno-Orovio A, Cherry EM, Evans SJ, Fenton FH. Basis for the Induction of Tissue-Level Phase-2 Reentry as a Repolarization Disorder in the Brugada Syndrome. BioMed Research International. 2015;2015:12.
30. Aiba T, Shimizu W, Hidaka I, et al. Cellular Basis for Trigger and Maintenance of Ventricular Fibrillation in the Brugada Syndrome Model: High-Resolution Optical Mapping Study. J Am Coll Cardiol. 2006;47:2074–2085. [PubMed: 16697328]

31. Park DS, Cerrone M, Morley G, et al. Genetically engineered SCN5A mutant pig hearts exhibit conduction defects and arrhythmias. The Journal of Clinical Investigation. 2015;125:403–412. [PubMed: 25500882]

32. Soh H, Park C-S. Localization of Divalent Cation-Binding Site in the Pore of a Small Conductance Ca2+-Activated K+ Channel and Its Role in Determining Current-Voltage Relationship. Biophys J. 2002;83:2528–2538. [PubMed: 12414687]

33. Weber CR, Piacentino V 3rd, Ginsburg KS, Houser SR, Bers DM. Na(+)-Ca(2+) exchange current and submembrane [Ca(2+)] during the cardiac action potential. Circ Res. 2002;90:182–189. [PubMed: 11834711]

34. Hegyi B, Bossuyt J, Griffiths LG, et al. Complex electrophysiological remodeling in postinfarction ischemic heart failure. Proceedings of the National Academy of Sciences. 2018;115:E3036–E3044.

35. Verkerk AO, Veldkamp MW, Baartscheer A, et al. Ionic Mechanism of Delayed Afterdepolarizations in Ventricular Cells Isolated From Human End-Stage Failing Hearts. Circulation. 2001;104:2728–2733. [PubMed: 11723027]

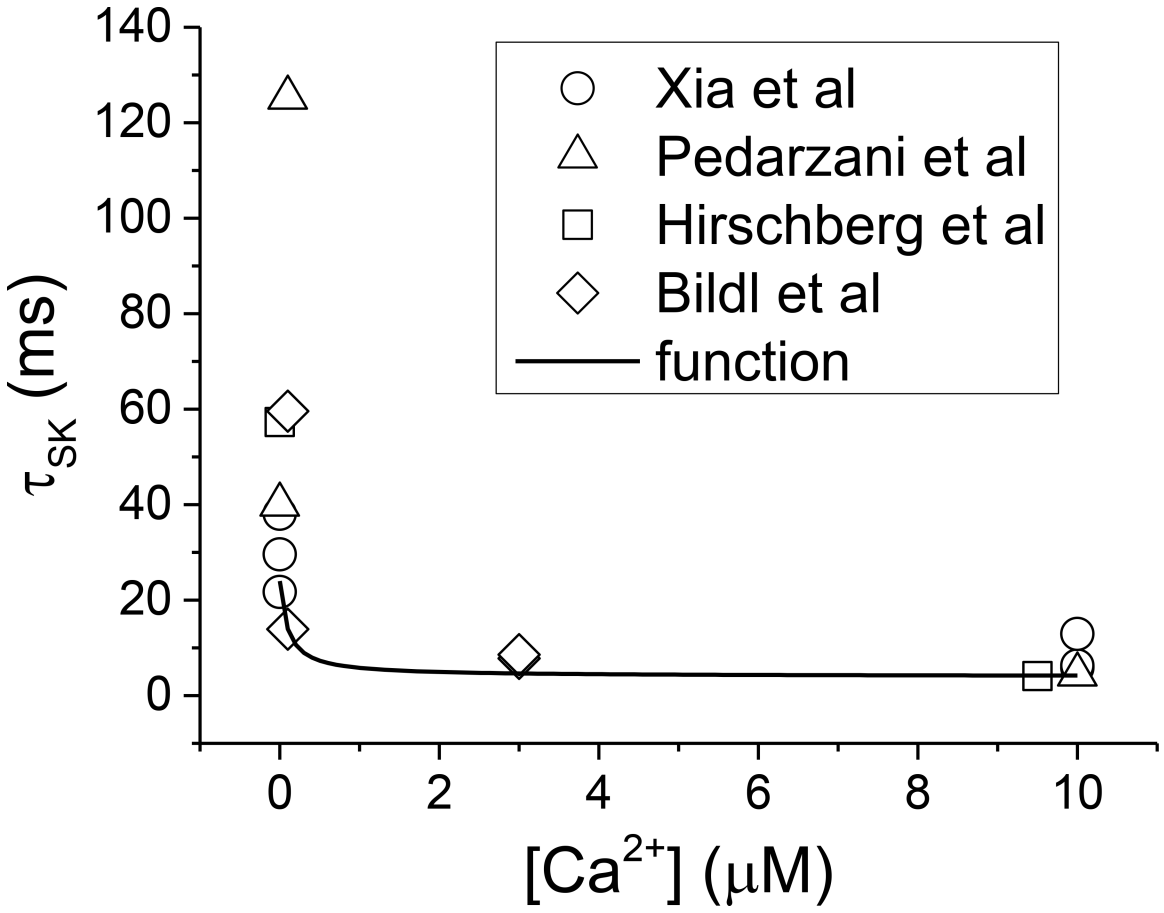

Figure 1. τ_{sk} versus intracellular Ca^{2+} concentration.

Different symbols are data from different experiments.[10–13] The line is a plot of the mathematical model Eq.6 with τ_0=4 ms and τ_1=20 ms.

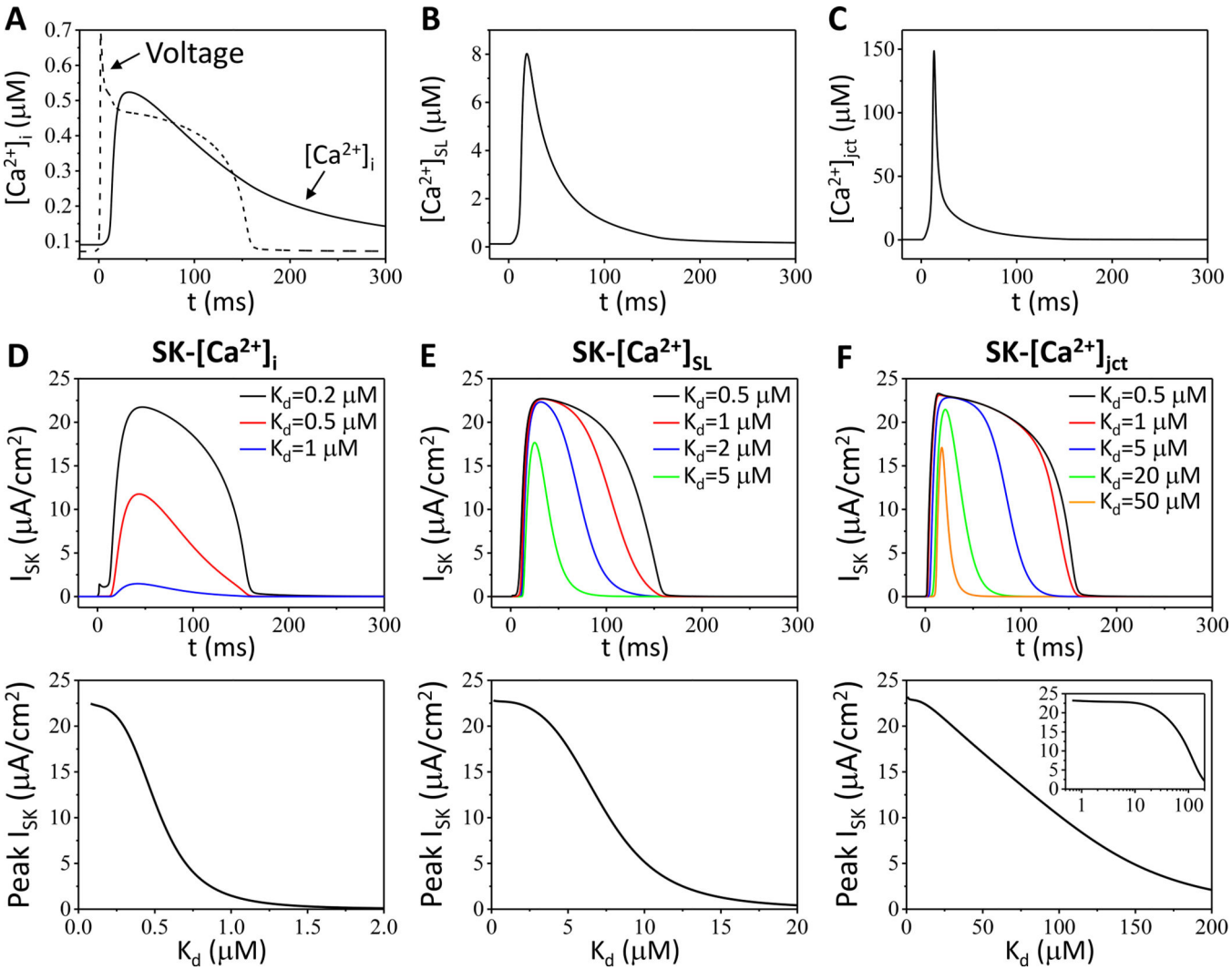

Figure 2. Ca^{2+} transients in different compartments of the Shannon-Bers model and dependence of I_{SK} properties on SK channel localization.

A. Dash line is the AP in the Shannon-Bers rabbit ventricular AP model [18]. Solid line is the bulk cytosolic Ca^{2+} concentration ($[Ca^{2+}]_i$) during the AP. **B**. Subsarcolemmal Ca^{2+} concentration ($[Ca^{2+}]_{SL}$) during the AP. **C**. Junctional Ca^{2+} concentration ($[Ca^{2+}]_{jct}$) during the AP. **D**. I_{SK} under AP clamp using the AP in A for different K_d values when the SK channels sense the bulk cytosolic Ca^{2+} (labeled as SK-$[Ca^{2+}]_i$). **E**. Same as A when the SK channels sense the subsarcolemmal Ca^{2+} (labeled as SK-$[Ca^{2+}]_{SL}$). **F**. Same as A when the SK channels sense the junctional Ca^{2+} (labeled as SK-$[Ca^{2+}]_{jct}$). $\mathbf{G}_{sk}$=0.25 pS/pF.

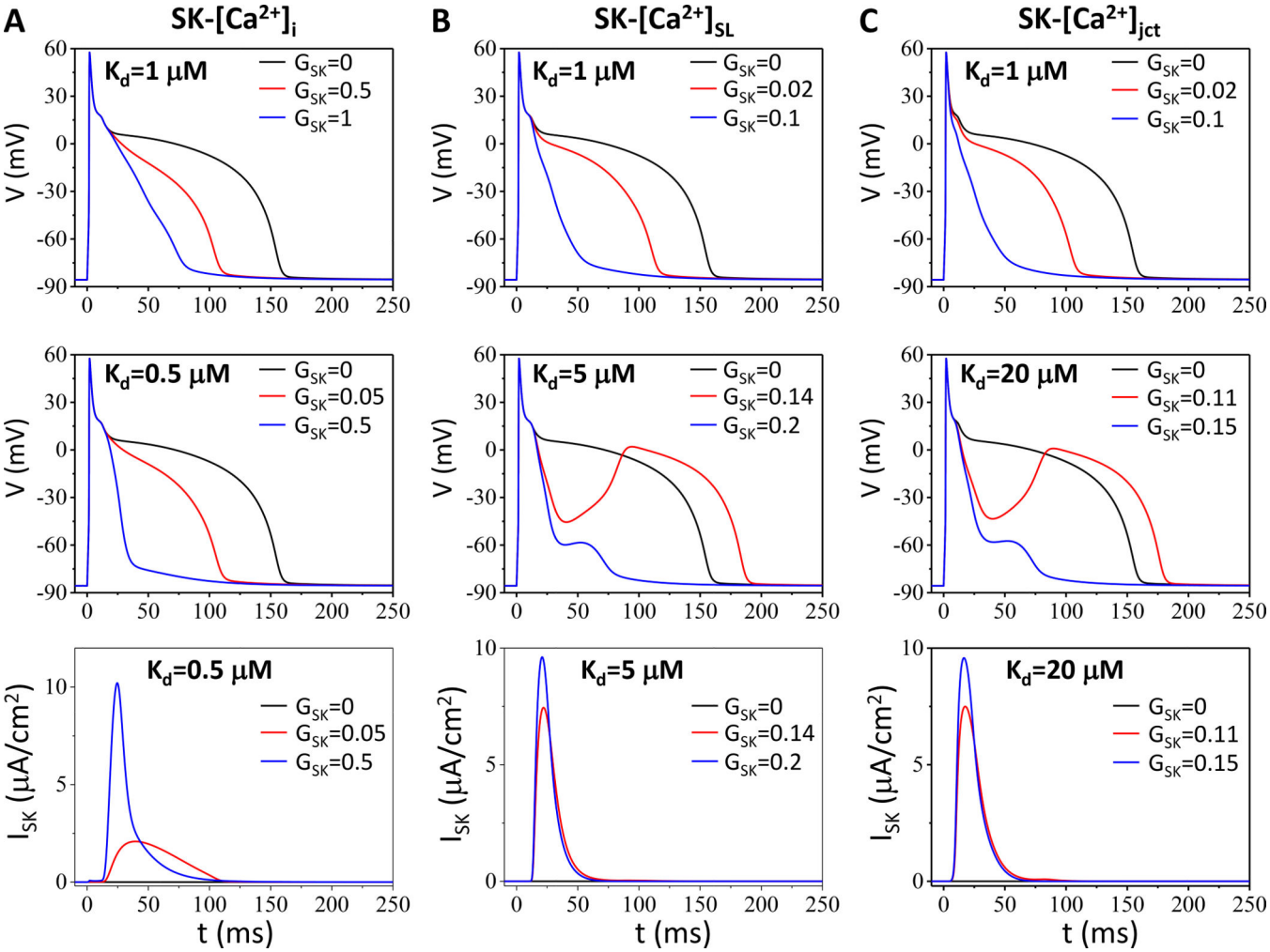

Figure 3. Effects of I_{SK} on AP morphology.

Shown are APs and I_{SK} for different K_d and G_{SK} as labeled. The unit of G_{sk} is mS/μF. **A**. SK-$[Ca^{2+}]_i$. **B**. SK-$[Ca^{2+}]_{SL}$. **C**. SK-$[Ca^{2+}]_{jct}$.

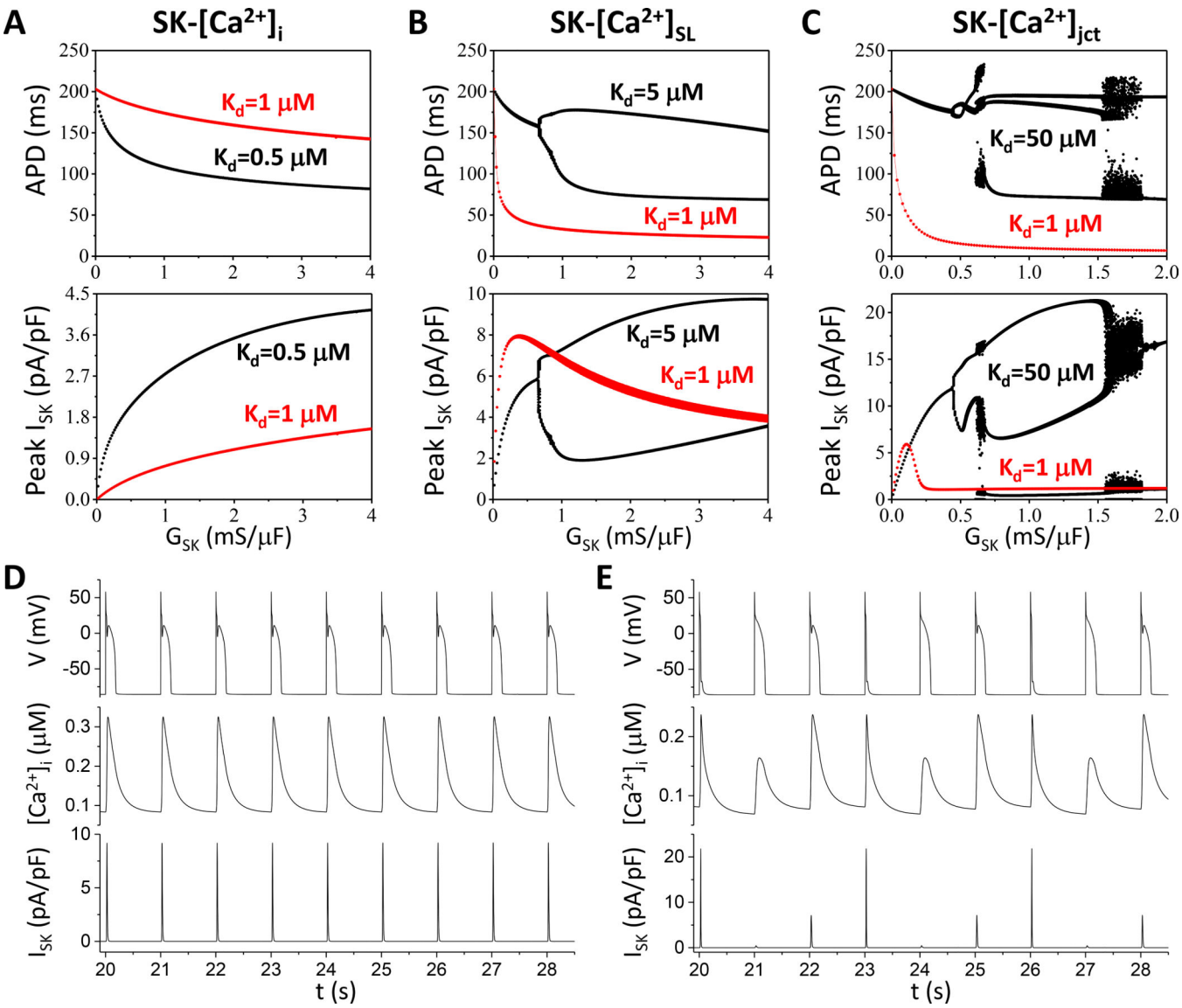

Figure 4. I_{SK} promotes complex APD dynamics.

A. APD and peak I_{SK} versus G_{SK} for SK-$[Ca^{2+}]_i$ with K_d=0.5 μM. **B**. APD and peak I_{SK} versus G_{SK} for SK-$[Ca^{2+}]_{SL}$ with K_d=5 μM. **C**. APD and peak I_{SK} versus G_{SK} for SK-$[Ca^{2+}]_{jct}$ with K_d=50 μM. In these panels, which are called bifurcation diagrams, APDs and peak I_{SK} from 60 beats are plotted for each G_{SK} values. The cells are paced with a pacing cycle length 1000 ms. **D**. Voltage trace, $[Ca^{2+}]_i$, and I_{SK} for G_{sk}=0.25 mS/μF for the case in C showing stable APD. **E**. Voltage trace, $[Ca^{2+}]_i$, and I_{SK} for G_{sk}=1 mS/μF for the case in C showing a period-3 behavior (an ABCABC... pattern in AP morphology and APD). Similar period-3 patterns was observed in experiments by Lukas and Antzelevitch[22] and by Morita et al[23], which were known to be caused by I_{to}.

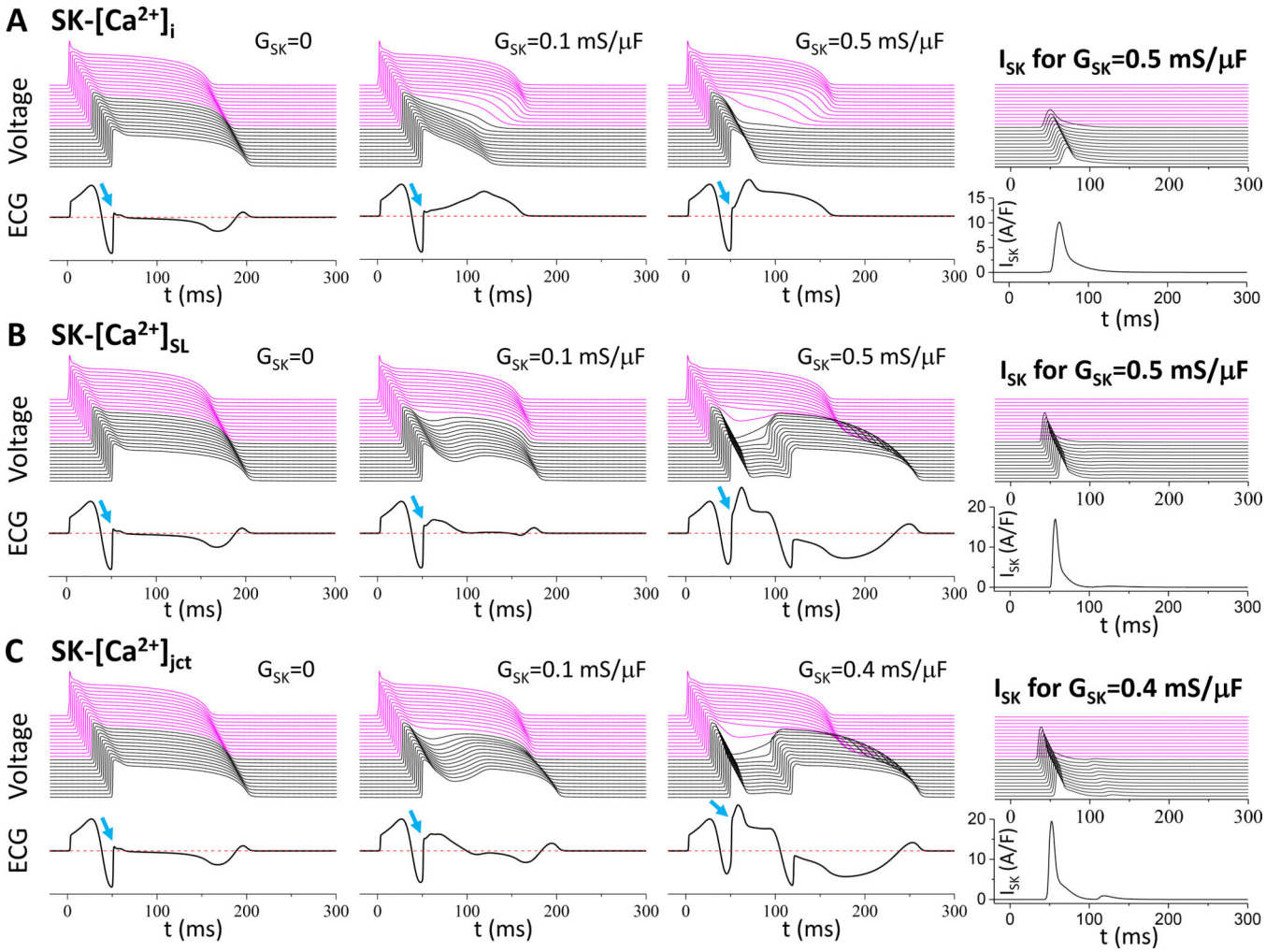

Figure 5. I_{sk} promotes J-wave elevation and P2R in a 1D cable with transmural heterogeneities.
The cable length is 200 cells. G_{sk} was set to 0 in the first half of the cable (100 cells, magenta) and a nonzero value (as labeled in each panel) uniformly in the second half (black), which was then increased to increase the heterogeneity. For all the 1D cable simulations, a single stimulus was given (t=0 ms) after the system reached the steady-state resting state. Upper panels: 3D (V-space-time) plots of voltage for three different G_{sk}. Lower panels: Pseudo-ECGs for each case. Arrows mark the J-points. The rightmost panels are the 3D plots of I_{SK} in whole cable (upper)and plots of I_{SK} from one cell in the second half of the cable for the largest G_{sk} for each SK channel localization. **A**. The SK channels sense the bulk cytosolic Ca^{2+}. K_d=0.5 μM. **B**. The SK channels sense the subsarcolemmal Ca^{2+}. K_d=5 μM. **C**. The SK channels sense the junctional Ca^{2+}. K_d=20 μM.

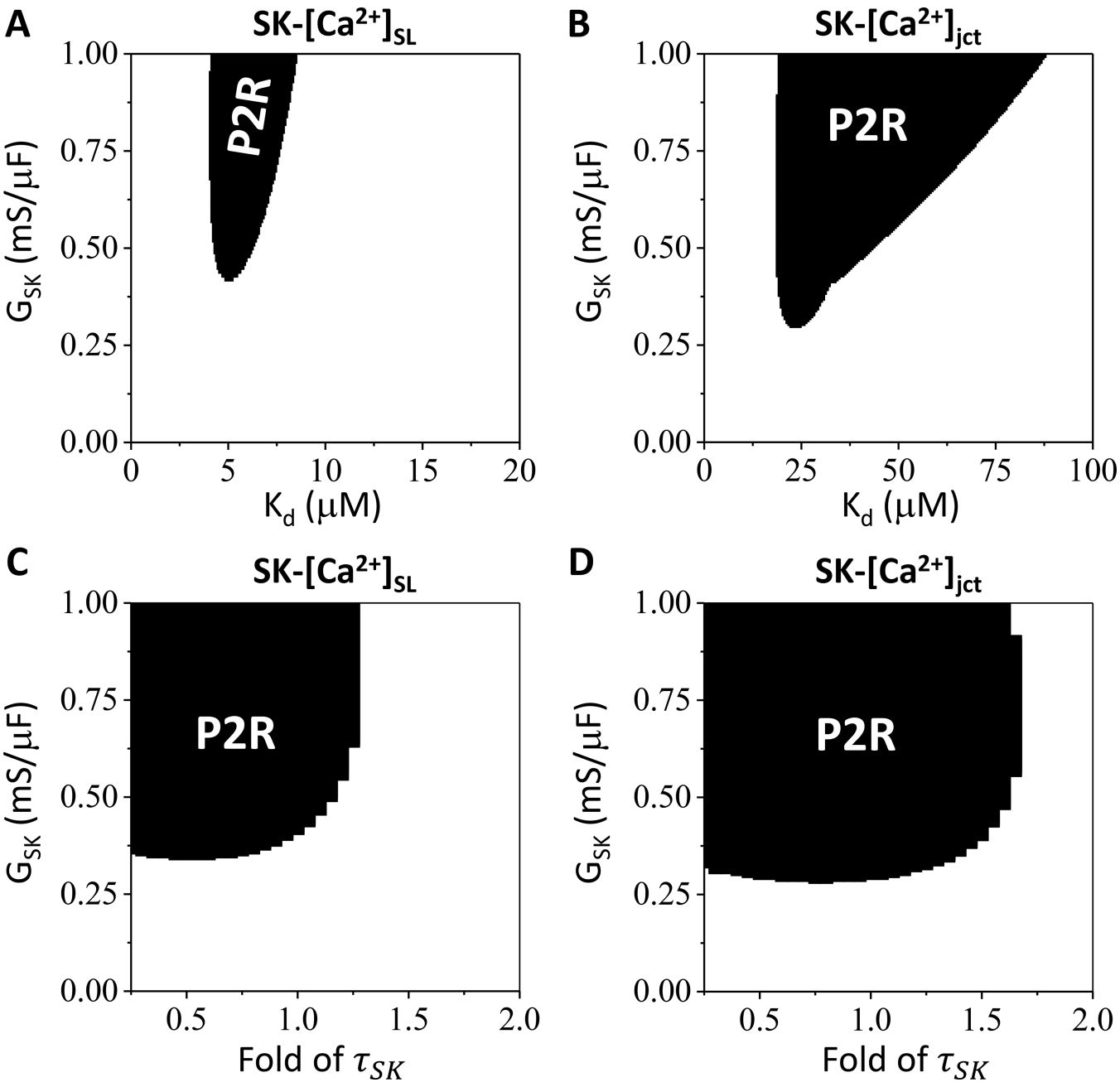

Figure 6. Effects of G_{SK}, K_d, and t_{SK} on P2R.

Shown are the P2R region in the combination of G_{sk} and K_d or G_{sk} and τ_{SK}. The same G_{sk} heterogeneities and pacing protocols as in Fig.5 were used. **A** and **C**. The SK channels sense the subsarcolemmal Ca^{2+}. **B** and **D**. The SK channels sense the junctional Ca^{2+}.

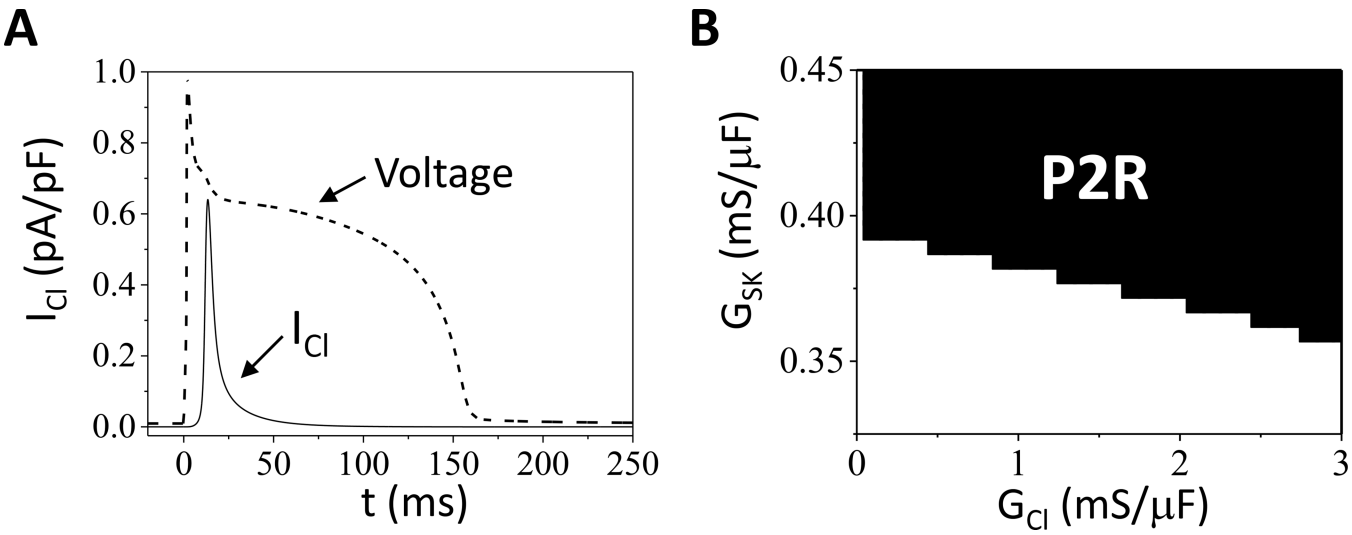

Figure 7.

Effects of I_{Cl} on P2R. **A**. I_{Cl} (solid line) under AP clamp (dashed line). We modified the I_{Cl} formulation (see Eq.74 in the Shannon-Bers paper[18]) to: $I_{Cl} = Fx_{Cl}\frac{G_{Cl}(V - E_{Cl})}{1 + \left(\frac{K_{dClCa}}{[Ca]_C}\right)^2}$, i.e., the Hill coefficient was changed from 1 to 2. The modification results in a spikier I_{Cl} which agrees better with the I_{Cl} profile measured in experiments by Hegyi et al.[34] **B**. P2R region versus G_{SK} and G_{Cl} for SK channels sense the subsarcolemmal Ca^{2+}. The same G_{SK} heterogeneities and pacing protocols as in Fig.5 were used. The G_{Cl} value was uniformly increased in the whole cable.